

The role of water models on the prediction of slip length of water in graphene nanochannels

Celebi, Alper Tunga; Nguyen, Chinh Thanh; Hartkamp, Remco; Beskok, Ali

DOI

[10.1063/1.5123713](https://doi.org/10.1063/1.5123713)

Publication date

2019

Document Version

Final published version

Published in

Journal of Chemical Physics

Citation (APA)

Celebi, A. T., Nguyen, C. T., Hartkamp, R., & Beskok, A. (2019). The role of water models on the prediction of slip length of water in graphene nanochannels. *Journal of Chemical Physics*, 151(17), Article 5123713. <https://doi.org/10.1063/1.5123713>

Important note

To cite this publication, please use the final published version (if applicable). Please check the document version above.

Copyright

Other than for strictly personal use, it is not permitted to download, forward or distribute the text or part of it, without the consent of the author(s) and/or copyright holder(s), unless the work is under an open content license such as Creative Commons.

Takedown policy

Please contact us and provide details if you believe this document breaches copyrights. We will remove access to the work immediately and investigate your claim.

Green Open Access added to TU Delft Institutional Repository

'You share, we take care!' – Taverne project

<https://www.openaccess.nl/en/you-share-we-take-care>

Otherwise as indicated in the copyright section: the publisher is the copyright holder of this work and the author uses the Dutch legislation to make this work public.


The role of water models on the prediction of slip length of water in graphene nanochannels

Cite as: J. Chem. Phys. **151**, 174705 (2019); <https://doi.org/10.1063/1.5123713>

Submitted: 08 August 2019 . Accepted: 15 October 2019 . Published Online: 05 November 2019

Alper Tunga Celebi , Chinh Thanh Nguyen , Remco Hartkamp , and Ali Beskok 

COLLECTIONS

 This paper was selected as Featured



View Online



Export Citation



CrossMark

ARTICLES YOU MAY BE INTERESTED IN

[A general purpose model for the condensed phases of water: TIP4P/2005](#)

The Journal of Chemical Physics **123**, 234505 (2005); <https://doi.org/10.1063/1.2121687>

[Multi-scale dynamics at the glassy silica surface](#)

The Journal of Chemical Physics **151**, 174502 (2019); <https://doi.org/10.1063/1.5123228>

[Shear force measurement of the hydrodynamic wall position in molecular dynamics](#)

The Journal of Chemical Physics **151**, 041103 (2019); <https://doi.org/10.1063/1.5111966>

Lock-in Amplifiers
... and more, from DC to 600 MHz



The role of water models on the prediction of slip length of water in graphene nanochannels

Cite as: J. Chem. Phys. 151, 174705 (2019); doi: 10.1063/1.5123713

Submitted: 8 August 2019 • Accepted: 15 October 2019 •

Published Online: 5 November 2019



View Online



Export Citation



CrossMark

Alper Tunga Celebi,^{1,a)}  Chinh Thanh Nguyen,²  Remco Hartkamp,¹  and Ali Beskok² 

AFFILIATIONS

¹Process and Energy Department, Delft University of Technology, Leeghwaterstraat 39, 2628 CB Delft, The Netherlands

²Lyle School of Engineering, Southern Methodist University, 3101 Dyer Street, Dallas, Texas 75205, USA

^{a)}Author to whom correspondence should be addressed: a.t.celebi-1@tudelft.nl. Tel.: +31(0)152783884.

ABSTRACT

Slip lengths reported from molecular dynamics (MD) simulations of water flow in graphene nanochannels show significant scatter in the literature. These discrepancies are in part due to the used water models. We demonstrate self-consistent comparisons of slip characteristics between the SPC, SPC/E, SPC/Fw, TIP3P, TIP4P, and TIP4P/2005 water models. The slip lengths are inferred using an analytical model that employs the shear viscosity of water and channel average velocities obtained from nonequilibrium MD simulations. First, viscosities for each water model are quantified using MD simulations of counterflowing, force-driven flows in periodic domains in the absence of physical walls. While the TIP4P/2005 model predicts water viscosity at the specified thermodynamic state with 1.7% error, the predictions of SPC/Fw and SPC/E models exhibit 13.9% and 23.1% deviations, respectively. Water viscosities obtained from SPC, TIP4P, and TIP3P models show larger deviations. Next, force-driven water flows in rigid (cold) and thermally vibrating (thermal) graphene nanochannels are simulated, resulting in pluglike velocity profiles. Large differences in the flow velocities are observed depending on the used water model and to a lesser extent on the choice of rigid vs thermal walls. Depending on the water model, the slip length of water on cold graphene walls varied between 34.2 nm and 62.9 nm, while the slip lengths of water on thermal graphene walls varied in the range of 38.1 nm–84.3 nm.

Published under license by AIP Publishing. <https://doi.org/10.1063/1.5123713>

I. INTRODUCTION

Liquid transport in nanoscale confinements is of great importance in various applications, ranging from drug delivery¹ to water desalination^{2–5} and biosensing.⁶ As the size of a conduit decreases down to the nanoscale, interfacial phenomena between liquid molecules and wall atoms become prominent, which leads to deviations from classical no-slip boundary conditions.⁷ For hydrophobic surfaces, a finite slip velocity is observed at the interface. This slippage typically is quantified by a slip length, which is the extrapolated distance to the wall at which the tangential velocity component vanishes. Although recent advances in nanofabrication techniques allow the utilization of nanometer-sized channels for nanofluidic applications,^{8–10} accurate slip length measurements are still experimentally challenging and expensive.¹¹ Alternatively, atomistic simulations can be employed to predict slip lengths at lower cost. Various molecular dynamics (MD) studies in the literature have focused on determining slip lengths of deionized water in graphene

nanochannels.^{12–17} Reported slip lengths in these MD-based studies are scattered in the range of 10 nm–100 nm. These variations are caused by several differences between the simulation models in these studies. Perhaps the most important difference is the intrinsic interaction parameters between the water models.

Hundreds of water models have been proposed in the literature, varying in interaction parameters, the number of charged sites, polarizability, and their cold or flexible structure.¹⁸ These variables can significantly influence the resulting microstructure and dynamics simulated water flows. For example, it was shown that hydrogen bond formation is highly dependent on the water model.¹⁹ TIP4P/2005 was found to exhibit stronger hydrogen bonding networks than SPC, SPC/E, and TIP4P. Stronger hydrogen bonding networks are associated with a higher viscosity of water. Differences between the properties of water models also affect transport in nanochannels, where velocity profiles can show different magnitudes and shapes with distinct slip velocities at the solid-liquid interface. The main objective of this study is to investigate the influence

of water models on the prediction of water slip length in nanoscale confinements. Another goal of the present study is to understand the role of wall's thermal vibrations on the slip length of water in nanochannels. We perform nonequilibrium MD simulations of some of the most widely used water models, including SPC, SPC/E, SPC/Fw, TIP3P, TIP4P, and TIP4P/2005, in graphene nanochannels. To the best of our knowledge, this is the first systematic study focusing on the slip behavior of different water models in nanochannels.

This study further distinguishes itself in providing a meticulous viscosity characterization, which is mandatorily required in calculating slip lengths. Viscosity can be calculated from MD simulations using various methods, such as the Green-Kubo formalism,^{20–23} Couette shear flow simulations,^{23–26} periodic perturbation method,^{24,27} Stokes-Einstein relation,^{28,29} transient-time correlation function,³⁰ and reverse nonequilibrium method,^{31,32} each with their strengths and limitations. Backer *et al.* presented an alternative approach that is based on counterflowing Poiseuille flows without the use of explicit boundaries.³³ This approach is more favorable in terms of providing high accuracy, good statistics, ease of implementation, and a relatively short convergence time.^{33,34} This latter method will be used here.

In this study, we take the following steps:

1. We will first carry out force-driven simulations of a periodic domain in the absence of any explicit walls to accurately determine the shear viscosity for each water model at a known thermodynamic state.
2. Next, force-driven flow simulations are carried out to obtain velocity profiles in cold and thermal nanochannels that are large enough to avoid size effects on viscosity and density.
3. Using the obtained viscosities and velocity profiles, slip lengths are calculated for the six water models considered here.

The remainder of this paper is structured as follows: Section II elaborates on the theory behind slip length calculation. In Sec. III, the details of the molecular dynamics simulation are explained. Then, the results of periodic domain and nanochannel simulations are presented and discussed.

II. THEORETICAL BACKGROUND

In this study, we simulate force-driven water flow in graphene-based planar nanochannels with different water models, as illustrated in Fig. 1. In order to theoretically assess liquid transport in nanochannels, we use the well-known principles of continuum fluid theory. The Navier-Stokes equation in the streamwise direction for a steady, incompressible, fully developed, force-driven Newtonian fluid flow between two parallel plates reduces to

$$\frac{d^2 u}{dz^2} = -\frac{f}{\mu}, \quad (1)$$

where $u(z)$ is the velocity field, μ is the viscosity of the liquid, and f is the applied body force in the streamwise (x) direction. Navier-type slip condition is employed at the liquid-solid interfaces ($z = 0$ and $z = h$), given by

$$u_l - u_w = \beta \frac{du}{dn}, \quad (2)$$

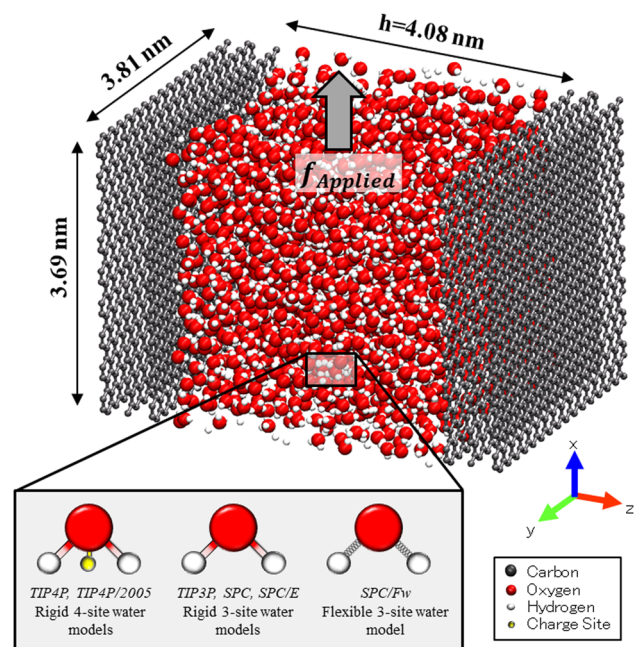


FIG. 1. Simulation domain and utilized water models.

where n is the outward normal into the liquid, β is the slip length, u_l is the liquid velocity, and u_w is the wall velocity. Assuming a constant slip length on both walls and assuming symmetry about the channel center, the water velocity profile between parallel plates with a separation distance of h is given by

$$u(z) = \frac{fh^2}{2\mu} \left(-\left(\frac{z}{h}\right)^2 + \left(\frac{z}{h}\right) \right) + \frac{fh\beta}{2\mu}. \quad (3)$$

The first term on the right-hand side of Eq. (3) is a measure for the curvature of the velocity profile, while the second term is the shift of the velocity profile due to slip between the fluid and the wall.³⁵ The latter term drops out in fully periodic simulations without physical walls. The fluid viscosity and slip length can be conveniently determined by fitting simulated velocity profiles to Eq. (3). However, the viscosity may be difficult to accurately determine from nanochannel systems, in which the bulk region can be small, and in the presence of hydrophobic interfaces, for which the variation in velocity can be much smaller than the slip velocity. Alternatively, we will calculate viscosity from homogeneous liquid simulations.

For nanochannel flows, a channel-height normalized slip length ($\beta^* = \beta/h$) is important for determining the shape of the velocity profile, where the focal length (distance between the vertex and focus) of the parabolic curve increases with increased β^* . The parabolic profile gradually becomes more flattened until “plug-like” velocity profiles are ultimately obtained.³⁶ To calculate the slip length for pluglike velocity profiles, we relate the conservation of linear momentum with the constitutive equation of shear stress for Newtonian fluids and the Navier-type slip given in Eq. (2).^{36,37} Wall shear (τ_w) is balanced with the total body force applied on water molecules based on conservation of linear momentum in the flow

direction as $\tau_w = \frac{\dot{h}}{2}$. This is then combined with the constitutive equation of $\tau_w = \mu \frac{du}{dz}$ and the slip equation as $u_s = \beta \frac{du}{dz}$. Here, the average channel velocities within an effective channel height ($h_e = h - 2L_0$) was used by introducing a slip plane on the first water density peak, where L_0 is the distance of the first density peak relative to the wall center.³⁶ The slip length is given by

$$\beta = \frac{2\mu u_s}{f_e h_e} \cong \frac{2\mu \bar{u}}{f_e h_e}, \quad (4)$$

where u_s and \bar{u} are the slip velocity and channel average velocity, respectively. The slip velocity is assumed to be equal to the average velocity for pluglike flows. For parabolic velocity profiles with finite slip length defined in Eq. (3), the above approximation of $u_s \cong \bar{u}$ results in an error of $1/[1 + 6(\beta/h_e)]$, which becomes less than 2% for $\beta/h_e > 9$. In Eq. (4), the slip length (β) associated with the slip plane is related to that on the channel wall (β_w) by $\beta = \beta_w + L_0$.³⁶ In this study, slip plane is defined at the first density peak because the liquid density near a surface reaches zero at the center of the first layer of wall molecules, and a typical gap of one molecular diameter ($\sim \sigma$) exists between the liquid slip plane and wall center plane. This is because liquid molecules cannot get any closer to the wall molecules due to their finite sizes. This physical gap is often comparable with the nanochannel dimensions.³⁸ It should be noted that the definition of the slip plane is versatile, ranging from the actual wall location to the first adsorption layer or at the Gibbs dividing plane as implemented in earlier works.^{39–45} In a very recent study, a nontraditional approach was used to identify the hydrodynamic wall position using the shear stress on the wall obtained from a single Poiseuille flow simulations.⁴⁶

III. MD SIMULATION SETTINGS

Six different water models are compared in this study. Rigid SPC, SPC/E, TIP3P, TIP4P, TIP4P/2005 models, and flexible SPC/Fw model are used. SPC type water models are three-site models providing simplicity and low computational.⁴⁷ TIP3P is also a three-site rigid water model that was developed to improve the energy and density representation of liquid water.⁴⁸ TIP4P and TIP4P/2005 are rigid four-site water models. The interaction parameters corresponding to these water models including well depth (ϵ_{OO}) and molecular diameter (σ_{OO}) between oxygen atoms are given in Table I.

The intermolecular interactions between all atomic species including van der Waals and electrostatic interactions were

described using Lennard-Jones (LJ) and long-range Coulomb potentials as follows:

$$V_{intermolecular}(r_{ij}) = 4\epsilon_{ij} \left[\left(\frac{\sigma_{ij}}{r_{ij}} \right)^{12} - \left(\frac{\sigma_{ij}}{r_{ij}} \right)^6 \right] + \frac{1}{4\pi\epsilon_0} \frac{q_i q_j}{r_{ij}}, \quad (5)$$

where ϵ_{ij} and σ_{ij} are the well depth and molecular diameter, respectively, ϵ_0 is the dielectric constant for vacuum, $q_{i(j)}$ are the partial charges, and r_{ij} is the distance between two atoms or charged sites. In Table I, ϵ_{OO} and σ_{OO} , respectively, refer to the well depth and molecular diameter for interacting oxygen atoms, while θ is the H–O–H angle and l_B is the O–H bond length. Four-site water models include a negatively charged, massless dummy atom along the bisector of the H–O–H angle separated from oxygen with a distance of l_{Om} . Furthermore, q_H and q_O are partial charges of hydrogen and oxygen atoms, respectively. In this study, a cutoff distance of 1 nm was used for all LJ and Coulomb potentials. The long-range electrostatic interactions were calculated using particle-particle-particle mesh (P³M) method with a root-mean-accuracy of 10^{-5} . For the flexible SPC/Fw model, harmonic bond stretching and bond angle vibration terms are included in the potential energy as follows:

$$V_{intramolecular} = \frac{1}{2} K_r (r - r_0)^2 + \frac{1}{2} K_\theta (\theta - \theta_0)^2, \quad (6)$$

where r_0 and θ_0 are equilibrium bond length and bending angle, respectively, and K_r and K_θ are the stretching and bending force constants of 4431.5 kJ/mol and 317.6 kJ/mol, respectively.⁵² In the rigid models, only intermolecular interactions are taken into consideration.⁵² SHAKE algorithm was used to keep bond lengths and angles constant in the rigid water models.⁵⁴

Figure 1 shows the simulation setup for the force-driven water flow through graphene nanochannels. The dimensions of the simulation domain are 3.69 nm and 3.81 nm in x - and y -directions, respectively. The channel height is 4.08 nm. The selection of the channel height is crucial because it must be large enough to avoid scale effect on viscosity. For liquids confined in channels narrower than 2–2.5 nm, liquid molecules can exhibit discrete molecular transport and the assumptions based on classical constitutive equations like Newton's law of viscosity might break down. Therefore, the local thermodynamic equilibrium and the description of macroscopic bulk properties of liquids, such as density and viscosity, become inaccurate at this scale. For example, Qiao and Aluru⁵⁵ showed in electro-osmotic flow simulations that a local constitutive relationship between shear stress and strain rate is not valid for channels smaller than 2 nm. A similar assessment on the ambiguity

TABLE I. Interaction parameters of the water models included in this study.

Water model	σ_{OO} (Å)	ϵ_{OO} (kJ/mol)	q_H (e)	q_O (e)	θ (deg)	l_B (Å)	l_{Om} (Å)
TIP3P ⁴⁸	3.1506	0.6364	0.4170	−0.8340	104.52	0.9572	N/A
TIP4P/2005 ⁴⁹	3.1589	0.7749	0.5564	−1.1128	104.52	0.9572	0.1546
TIP4P ⁵⁰	3.1537	0.6485	0.5200	−1.0400	104.52	0.9572	0.1500
SPC ⁵¹	3.1656	0.6503	0.4100	−0.8200	109.47	1.0000	N/A
SPC/Fw ⁵²	3.1656	0.6503	0.4100	−0.8200	113.24	1.0120	N/A
SPC/E ⁵³	3.1656	0.6503	0.4238	−0.8476	109.47	1.0000	N/A

of local viscosity was also indicated by an earlier study by Travis *et al.*⁵⁶ In this study, we used both rigid and thermal walls to explore the effect of thermal wall motion on the slip length. Thermostatting walls can affect the interfacial water structure and dynamics of liquids in nanochannels.^{38,57–59} It was reported that the flow rate of liquid methane in thermally vibrating graphene channels increased by 20% when compared with the results of cold walls.⁵⁷ In addition, Sam *et al.*⁶⁰ showed that the flow of SPC/E water in thermally vibrating carbon nanotubes is 12%–20% larger than the flow through cold carbon nanotubes. Accordingly, slip lengths are found to be proportionally larger for thermal channel walls.^{16,57} In the present study, the rigid (cold) walls composed of four A-B-A stacked graphene layers with a distance of 0.34 nm between the adjacent layers.⁶¹ To obtain a rigid wall model, the wall atoms were fixed at their initial positions.^{17,36,37} For thermally vibrating walls, we used four graphene layers, where the inner three graphene layers were thermostated using an NVT ensemble, while the most outer layers were fixed at their original positions. Periodic boundary conditions were applied in x - and y -directions, while the z -direction is bounded by the channel walls. To account for electrostatic interactions in the bound z -direction, we employed a correction term to the standard Ewald algorithm, which was proposed by Yeh and Berkowitz.⁶² Interaction parameters between wall atoms and water molecules were based on the earlier parameterization of experimental water/graphene contact angle measurements.⁶³ To recover a macroscopic contact angle of 86° , the well-depth parameter between carbon and oxygen atoms was systematically calibrated using the linear relation between the interaction energy and MD-predicted contact angles for droplets consisting of different number of molecules. Note that this linear relationship was required because of computational limitations in MD simulations, which make direct reproduction of the experimentally large water droplets impossible to simulate. However, wettability on a graphitic substrate is still controversial since experimental measurements showed large variations in the range of 30° – 127° .^{64–75} These large variations are possibly due to the effects of relative humidity, surface contaminations, utilized methods, or the number of graphene layers.^{64,67,71} The present study contains three graphene layers for cold walls and four graphene layers for thermal walls. The additional layers exhibit a negligible effect on the wettability because they are beyond the wall potential cutoff distance. The velocities of the water molecules in the system were initialized by a Gaussian distribution at 300 K. The number of water molecules in the simulation domain was 1862 for TIP4P/2005. For other water models, this number was changed by a maximum of 3 molecules to achieve the desired bulk density (997 kg/m^3) at the channel center. We first thermally equilibrated each system in a canonical (NVT) ensemble before applying any external force. Each system was equilibrated for 2 ns using a time step of 1 fs. Next, flow was induced by applying a constant body force to the water molecules in the x -direction. Temperature was kept constant using the Nosé-Hoover thermostat applied only to the degrees of freedom perpendicular to the flow direction. For flow cases, the characteristic time scale for momentum diffusion is determined as $t_d \approx \frac{h^2}{\nu}$, where ν is the kinematic viscosity and h is the channel height.³⁶ This gives an estimate for time required for flow to reach a steady state. We initially ran for 2 ns, which is equivalent to $12.5t_d$. An additional 30 ns was then run for data collection and statistical averaging. The domain was divided

into 1200 bins in the z -direction. All simulations were performed using Large-Scale Atomic/Molecular Massively Parallel Simulator (LAMMPS) package.⁷⁶

IV. RESULTS AND DISCUSSIONS

A. Viscosity calculation

Calculating the slip length of water in hydrophobic nanochannels using Eq. (4) requires knowledge of the viscosity of the fluid. To predict the viscosity of different water models, we simulated counterflows in a domain without any explicit boundaries.³³ In this method, we divided the simulation box into two identical subdomains, with both subdomains being subjected to equal body forces in opposite directions (Fig. 2). The flow was obtained by externally applied force to the center of each atom in a water molecule in the x -direction. The magnitude of the external force on each atom was set based on the atomic masses of oxygen and hydrogen to achieve a constant acceleration. The applied force for periodic water domain simulation was $1.5 \times 10^{-4} \text{ eV/\AA}$ independent of the water model. These counteracting forces constrain the liquid as if there are fictitious solid boundaries, creating parabolic velocity profiles with no-slip at the domain center and edges without inhomogeneous fluid density. To calculate the viscosities, the following procedure is used. First, MD-predicted velocity profiles of each subdomain of the periodic box are fitted to a second-order polynomial equation in the form of $u(z) = Az^2 + Bz + C$. Then, the A and B coefficients are compared with the analytical solution of Poiseuille flow between planar plates considering no-slip boundary conditions ($\beta = 0$) given by the following equation:³⁵

$$u(z) = \frac{fh^2}{2\mu} \left(-\left(\frac{z}{h}\right)^2 + \left(\frac{z}{h}\right) \right). \quad (7)$$

Viscosities are obtained by using the following relations:

$$\mu = -\frac{f}{2A} \quad \text{and} \quad \mu = -\frac{fh}{2B}. \quad (8)$$

Using this fitting method, one can calculate four different viscosity values.³⁵ Based on the two parabolic velocity profiles of

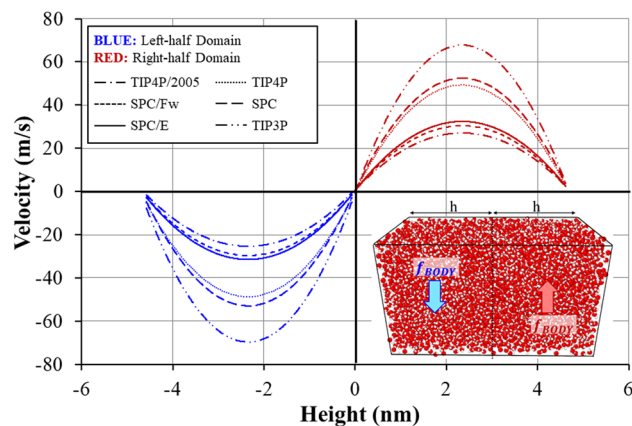


FIG. 2. Velocity profiles of counterforce driven water flow.

counteracting flows, μ_1 and μ_2 are obtained using coefficients of *A*, whereas μ_3 and μ_4 are calculated using coefficients of *B*. Then, their mean value is compared with the experimental viscosity of water ($\mu_{\text{exp}} = 853 \mu\text{Pa s}$ at $T = 300 \text{ K}$ and $\rho = 997 \text{ kg/m}^3$).

Figure 2 shows the velocity profiles of counteracting flows simulated with the six different water models in a periodic domain ($2h = 9.52 \text{ nm}$). Simulated systems are large enough so that viscosity calculations do not suffer from any size dependence.^{24,35} Each velocity profile has a parabolic shape but a different magnitude. The magnitude of the velocity profiles shows an increasing trend with the use of TIP4P/2005, SPC/Fw, SPC/E, TIP4P, SPC, and TIP3P water models, respectively. For example, considering the magnitude of the average velocities in the left and right domains as given in Fig. 2, the velocity for TIP3P is approximately 2.6 times greater than that for TIP4P/2005 under the same applied force. Average velocities are related to computed viscosities of the associated water models as listed in Table II. Among all water models, TIP4P/2005 has the highest viscosity with an average value of $838.8 \mu\text{Pa s}$. It presents the best performance in capturing experimental viscosity of water at 300 K with 1.7% deviation. This good viscosity reproduction of the TIP4P/2005 water model is mainly attributed to its ability in creating strong hydrogen bonds.¹⁹ SPC/Fw and SPC/E yield moderately acceptable predictions of the experimental viscosity value, whereas TIP4P, SPC, and TIP3P present poorer performance. The average viscosity of TIP3P ($319.1 \mu\text{Pa s}$) is approximately 62% off from its experimental value. Comparing the parameters of SPC/E and SPC, the former only has a slightly higher partial charge on its oxygen and hydrogen. This minor difference results in a self-polarization energy correction for the effective pair potentials of the SPC/E model and drastically changes the viscosity from $409.5 \mu\text{Pa s}$ to $655.1 \mu\text{Pa s}$.⁵² Furthermore, a viscosity of $734 \mu\text{Pa s}$ was found for SPC/Fw. This significantly higher viscosity than that of SPC can be a consequence of the introduced flexibility as well as the modified bond length and angle parameters. The flexible water model provides a more physical approach for handling polarization effects, by including harmonic stretching and bending terms to describe intramolecular interactions in addition to the intermolecular ones.^{52,77} Our viscosity results for the different water models are consistent with values reported in the literature.^{19–24,27,34,77}

For water flows in nanochannels, one must consider the effect of confinement on the viscosity. Multiple studies have showed that the viscosity of liquids in nanochannels with heights as large as 3 nm can be significantly larger than the shear viscosity in the bulk region.^{34,35,56,78} This is caused predominantly by the solid-fluid

interaction and the resulting inhomogeneous fluid density very close to a solid surface. Suk and Aluru studied the viscosity of water in CNTs as a function of nanotube diameter, showing that viscosity is substantially larger for narrow channels but reaches to the viscosity of SPC/E model in the bulk region for channel diameters larger than 2.6 nm .⁷⁸ Russo *et al.* found that the viscosity enhancement in nanoconfinement becomes more prominent with an increasing hydrophilicity of the channel walls, although variations in local viscosity exist also in hydrophobic channels.²⁶ Furthermore, Markestijn *et al.*³⁴ showed that the viscosities of several water models in a planar nanochannel separated by 4.3 nm distance are in good agreement with viscosities of associated water models without any explicit boundaries. We therefore specified a channel height large enough that scale effect on viscosity is negligible.^{17,37} It should be noted that several reports in the literature indicated spatially varying viscosities in nanochannels based on locally applied linear constitutive relationship between shear stress and strain rate.^{55,79–82} Especially the interfacial viscosity of water may differ from its value away from the walls. Despite these variations, velocity profiles obtained from MD simulations can be described using the Poiseuille flow relation with a constant “effective” viscosity. Ghorbanian and Beskok³⁵ computed liquid viscosity using parabolic velocity profiles. They reported that shear stresses away from the interfaces correlated well with the constitutive law for a Newtonian fluid for channel heights larger than 3.26 nm . However, the “effective” viscosity varied with the channel size and reached its thermodynamic value for channel heights larger than 50 nm . In the present study, we observe pluglike velocity profiles, where the calculation of viscosity from the velocity profile or using local shear stresses calculated from the MD data are prone to statistical errors mainly due to the very low strain rates (du/dz). Therefore, we refer to viscosity as a constant transport property obtained from the periodic counterflow simulations.

B. Nanochannel flow simulation for slip length calculation

Next, force-driven water flows in graphene nanochannels are simulated. Similar to the periodic domain simulations, flow was driven by a constant body force imposed on the water molecules in the x -direction. The magnitude of the external force on each atom was correlated with their atomic masses so that a constant acceleration is achieved. In Fig. 3, density distributions for different water models are shown. Each profile shows three dense fluid layers near

TABLE II. Viscosity of different water models by periodic box simulations. Experimental viscosity of water is $853 \mu\text{Pa s}$ at $T = 300 \text{ K}$ and $\rho = 997 \text{ kg/m}^3$.

Water model	μ_1 ($\mu\text{Pa s}$)	μ_2 ($\mu\text{Pa s}$)	μ_3 ($\mu\text{Pa s}$)	μ_4 ($\mu\text{Pa s}$)	μ_{AVE} ($\mu\text{Pa s}$)	Error (%)
TIP4P/2005	846.8	843.3	835.4	830.0	838.8	1.7
SPC/Fw	734.1	733.4	732.9	734.8	733.8	13.9
SPC/E	657.4	658.5	653.3	651.1	655.1	23.1
TIP4P	451.5	458.6	447.0	445.8	450.7	47.2
SPC	412.8	411.6	407.0	406.9	409.5	51.9
TIP3P	320.3	321.5	318.3	316.2	319.1	62.6

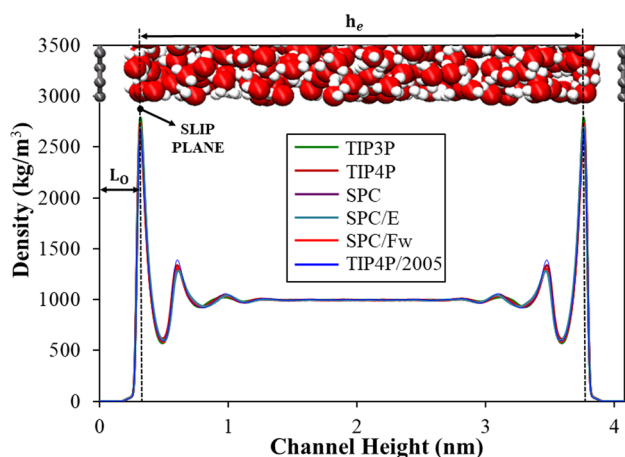


FIG. 3. Density distribution of water in graphene nanochannels obtained using different water models.

the wall and a prominent bulk region at the channel center.⁸³ For each water model, the density in the bulk region of the channel is 997 kg/m^3 and the fluid temperature is kept at 300 K.^{17,37} As seen in Fig. 3, the magnitudes and locations of the density peaks of different water models are very similar. We found that the first sharp density peaks are located approximately 0.32 nm (L_0) from the center of the wall atoms in the inner graphene layer, in agreement with previous reports.^{84–86} Notably, this distance can slightly differ depending on the thermostatting approach.⁶⁰

Next, we present the velocity profiles of water in rigid walls for different water models. For each case, flow was induced by body forces acting in the x -direction. In Fig. 4, each velocity profile exhibits pluglike behavior with a large velocity slip at the interfaces. This behavior is mainly related to the low friction between the water and graphene, due to the combined effects of high atomic density and smooth surface of the graphene and the weak liquid-solid interactions.³⁸ Note that both periodic water box simulations

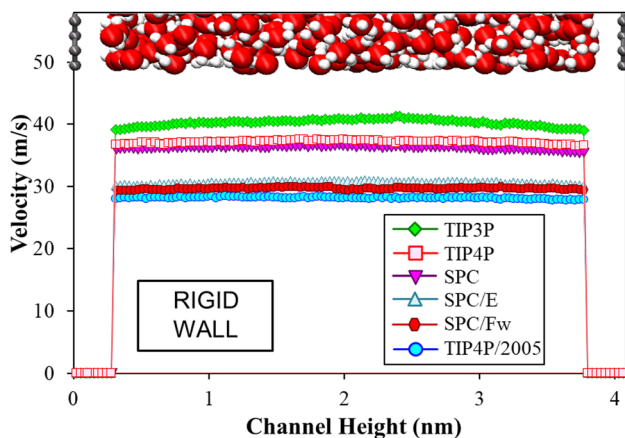


FIG. 4. Velocity profiles of water in rigid graphene channels for six different water models.

and nanochannel simulations were carried out in the linear response regime. This linear regime was determined by systematically analyzing the average velocities as a function of driving force (not shown for brevity).¹⁷ For nanochannel simulations, we observe that the average channel velocities linearly increase with externally applied force up to 50 m/s . Beyond this value, nonlinear variations in the flow rate began to appear, which leads to inaccurate slip lengths.⁸⁷ Our results reveal that the magnitude of velocities depends on the water model with an increasing trend of TIP4P/2005, SPC/Fw, SPC/E, SPC, TIP4P, and TIP3P. TIP4P/2005 shows the smallest average channel velocity (28.3 m/s), while TIP3P shows the maximum average velocity (40.7 m/s). SPC/Fw, SPC/E, SPC, and TIP4P, respectively, range between these two values. One of the important factors is the viscosity of the associated water model. The highest viscosity of the TIP4P/2005 model results in the lowest velocity, while the lowest viscosity of TIP3P exhibits the fastest flow under equal driving forces. Interestingly, the viscosity is not the only factor influencing the velocity profiles in graphene nanochannels. For instance, the SPC water model shows slightly lower velocity profiles than TIP4P, whereas the former exhibits a lower viscosity. A similar anomaly between the viscosities and diffusion coefficients of SPC and TIP4P water models was observed in an earlier study.⁸⁸ Furthermore, we found that the viscosity of TIP4P/2005 is 2.6 times larger than TIP3P, whereas the ratio of their average velocities in nanochannels is only 1.4. The difference is attributed to the contribution of the slip.

In Fig. 5, velocity profiles of different water models in thermal graphene channels are shown. Note that the flow was driven by the same body forces as in the rigid (cold) wall simulations. Thermostatting the walls affects the flow of different models of water differently. The average velocities of water in thermal graphene channels exhibit 10%–33% increase compared with the respective rigid walls. The lowest change is obtained in the case of TIP3P water model, while the highest is obtained for TIP4P/2005. In the case of thermal walls, the velocity profiles corresponding to the various water models show a different ordering than those of rigid walls. As shown in Fig. 5, SPC/E water model has the lowest velocity in the thermal channel,

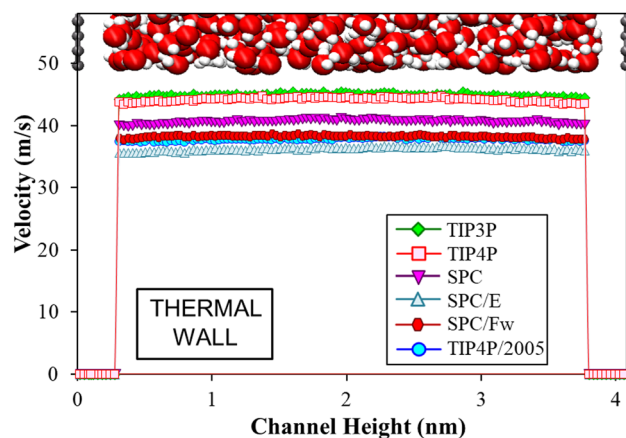


FIG. 5. Velocity profiles of water in thermal graphene channels for six different water models.

TABLE III. Variation in water slip lengths in rigid and thermal graphene nanochannels for different water models using simulated viscosity (Sim. Visc.) and experimental viscosity (Expt. Visc.). The present results are compared with the slip lengths obtained from earlier equilibrium (EMD) and non-equilibrium (NEMD) molecular dynamics simulations in literature.

Reference study	Slip length (nm)							Viscosity ($\mu\text{Pa s}$)	Method
	TIP4P/2005	TIP4P	TIP3P	SPC/E	SPC/Fw	SPC	TIP5P		
Present (Sim. Visc.) rigid walls	62.9	44.6	34.2	53.3	57.8	39.4	...	Table II	Based on average velocities using Eq. (4) (NEMD)
Present (Sim. Visc.) thermal walls	84.3	53.0	38.1	63.1	74.4	44.2	...	Table II	Based on average velocities using Eq. (4) (NEMD)
Present (Expt. Visc.)	64.4	84.4	91.5	69.5	67.4	81.9	...	853	Based on average velocities using Eq. (4) (NEMD)
Kannam <i>et al.</i> ¹⁴	60 ± 5	750	Based on friction coefficient obtained from EMD simulations
Kannam <i>et al.</i> ¹⁴	62 ± 5	750	Based on velocity profiles obtained from Poiseuille flow simulations (NEMD)
Kannam <i>et al.</i> ¹⁴	58 ± 8	750	Based on velocity profiles obtained from Couette flow simulations (NEMD)
Xiong <i>et al.</i> ¹⁵	54	820	Based on friction coefficient obtained from Green-Kubo simulations (EMD)
Thomas and McGaughey ¹²	30	890	Based on friction coefficient obtained from Green-Kubo simulations (EMD)
Thomas and McGaughey ¹²	31	890	Based on velocity profiles obtained from Poiseuille flow simulations (NEMD)
Sam <i>et al.</i> ¹⁶	64–69	704	Based on friction coefficient obtained from EMD simulations
Sam <i>et al.</i> ¹⁶	66–68	704	Based on velocity profiles obtained from Poiseuille flow simulations (NEMD)
Borg <i>et al.</i> ⁸⁹	61	855	N/A
Wei <i>et al.</i> ⁹⁰	48	729	Based on friction coefficient obtained from Green-Kubo simulations (EMD)
Falk <i>et al.</i> ¹³	80	N/A	Based on friction coefficient obtained from both EMD and NEMD simulations
Falk <i>et al.</i> ¹³	80	N/A	Based on friction coefficient obtained from both EMD and NEMD simulations
Ramos-Alvarado <i>et al.</i> ⁴¹	29	792	Based on friction coefficient obtained from Green-Kubo simulations (EMD)
Wagemann <i>et al.</i> ⁵⁹	50	729	Based on velocity profiles obtained from Poiseuille flow simulations (NEMD)
Gu and Chen ⁹¹	77	N/A	Based on velocity profiles obtained from Couette flow simulations (NEMD)
Koumoutsakos <i>et al.</i> ⁹²	63	N/A	Based on velocity profiles obtained from Couette flow simulations (NEMD)

while this was the case for TIP4P/2005 water model in the rigid channel. SPC/E is followed by TIP4P/2005, SPC/Fw, SPC, TIP4P, and TIP3P. Furthermore, whereas the curvature seemed to vary between models in the rigid (cold wall) channel, the curvature seems to be more consistent between the water models in the thermal channel (and less pluglike than for rigid walls, except for the TIP3P water model).

The shape of a velocity profile plays a critical role in the determination of the slip length in nonequilibrium MD simulations. Velocity profiles for hydrophilic channels have strong parabolic component with small slip length at interface, which can be extracted from polynomial curve fitting.³⁵ However, velocity profiles in hydrophobic channels typically exhibit very weak parabola that curve fitting to this results in a large statistical error.¹⁴ Therefore, the slip length for such systems was calculated using Eq. (4), which is extensively formulized in Sec. II. Table III gives an overview of slip lengths calculated in this study compared with the values reported in the literature, which are obtained within the validity of linear response regime. Our results are comparable with several values reported in the literature. We note, however, that there is no other study in the literature that calculates the slip length for all these water models in the same system, which is needed to make a self-consistent comparison between the slip characteristics of different water models. It is important to point out that the slip length of water confined between parallel plates is size independent for 3-nm channels and larger. Sam *et al.*¹⁶ showed that slip length of water in graphene channels exhibit no strong dependency on channel height using EMD and NEMD simulations. Ramos-Alvarado *et al.*⁴¹ also reported constant slip lengths for water-graphene system as a function of the channel height. Considering water flow in rigid walls, we find slip lengths in the range of 34.2–62.9 nm using the viscosities of the water models given in Table II, TIP4P/2005 shows the strongest slip, while TIP3P shows the least slip. Slip lengths of SPC, TIP4P, SPC/E, and SPC/Fw show an increasing order, respectively. Furthermore, one can notice that the velocity profile of the TIP3P water model is slightly parabolic. Fitting to this parabola, as explained in earlier studies,^{35,36} we find the slip length as 33.4 nm, which perfectly agrees with the result (34.2 nm) obtained using Eq. (4). In Table III, the slip length of different water models on thermal graphene walls is also provided, where the slip length values are increased by 10%–33%. We found that the slip lengths on thermal walls vary between 38.1 nm and 84.3 nm for the TIP3P and TIP4P/2005 water models, respectively. Slip length of SPC/E water model shows an increase of 19% when compared with that of cold wall predictions. This agrees with results reported by Sam *et al.*¹⁶ It should be also noted that the ordering of slip length as a function of the used water model remains same with rigid wall case. In Table III, we also provide a second slip length description which utilizes the experimental viscosity ($\mu_{TD} = 853 \mu\text{Pa s}$) of water at $T = 300 \text{ K}$ instead of the viscosity of the associated water model. This is important to better distinguish the effect of viscosity on slip lengths. For example, slip lengths for TIP4P and TIP3P water models are, respectively, calculated as 84.4 nm and 91.5 nm using experimental viscosity, whereas values of 34.4 nm and 43.7 nm are found when using computationally obtained viscosities. TIP4P/2005 water model shows similar values for both definitions since it has the highest capability of this water model to reproduce bulk water properties at specified thermodynamic conditions. One can notice in Table III

that many studies considered SPC/E water models in their simulations mainly due to its simplicity and low computational cost. In addition, the reported slip length values for the same water models are generally close to each other, although small discrepancies exist. We have shown here that the calculated slip length depends strongly on the water model used, as well as on the viscosity value, since viscosity is used as a fitting parameter for the slip length. Besides, several algorithmic or physical details such as liquid-wall interaction parameters, thermal/cold wall approximation, domain size, efficiency of thermostats, nonlinear flow contributions, and slip calculation methodology are some of the reasons for those small discrepancies.

V. CONCLUSION

In this work, we systematically compared slip lengths of six commonly used water models, namely, SPC, SPC/E, SPC/Fw, TIP3P, TIP4P, and TIP4P/2005, by performing force-driven flow simulations in rigid and thermal graphene nanochannels. Slip length calculations require knowledge of the fluid shear viscosity, which was obtained from counter Poiseuille flow simulations in a periodic water box. Of the water models considered here, TIP4P/2005 gives the best prediction of viscosity, within 1.7% deviation from the experimental value, while those obtained from SPC/Fw and SPC/E are also moderately accurate. TIP4P, SPC, and TIP3P show poorer performance in reproducing viscosity at specified thermodynamic conditions. Pluglike flow velocity profiles were observed for all water models for cold and thermally vibrating graphene nanochannels. Using these velocity profiles and predicted viscosities, slip lengths of water on cold walls are found approximately in the range of 34 nm–63 nm, where the TIP4P/2005 water model results in the largest slip length and TIP3P model has the smallest slip length. For thermally vibrating nanochannels, the slip length of TIP4P/2005 model (84.3 nm) is more than twice that of TIP3P model (38.1 nm). Slip lengths of other water models are between these two values. For both cold and thermal walls, slip length exhibits an increasing trend using TIP3P, SPC, TIP4P, SPC/E, SPC/Fw, and TIP4P/2005 models. In addition, slip lengths are calculated using thermodynamic viscosity instead of MD-predicted viscosities, where TIP4P/2005 model exhibits similar slip for these two descriptions, since it well predicts the experimental viscosity.

REFERENCES

- 1 A. Angelova, B. Angelov, S. Lesieur, R. Mutafchieva, M. Ollivon, C. Bourgaux, R. Willumeit, and P. Couvreur, *J. Drug Delivery Sci. Technol.* **18**(1), 41–45 (2008).
- 2 D. Cohen-Tanugi and J. C. Grossman, *Nano Lett.* **12**(7), 3602–3608 (2012).
- 3 C. T. Nguyen and A. Beskok, *J. Chem. Phys.* **149**(2), 024704 (2018).
- 4 C. T. Nguyen and B. Kim, *Int. J. Precis. Eng. Manuf.* **17**(4), 503–510 (2016).
- 5 C. T. Nguyen, M. Barisik, and B. Kim, *AIP Adv.* **8**(6), 065003 (2018).
- 6 R. Karnik, K. Castelino, and A. Majumdar, *Appl. Phys. Lett.* **88**(12), 123114 (2006).
- 7 R. J. Hunter, *Foundations of Colloid Science* (Oxford University Press, 2001).
- 8 C. Duan, W. Wang, and Q. Xie, *Biomicrofluidics* **7**(2), 026501 (2013).
- 9 Q. Xie, F. Xin, H. G. Park, and C. Duan, *Nanoscale* **8**(47), 19527–19535 (2016).
- 10 W. Jung, J. Kim, S. Kim, H. G. Park, Y. Jung, and C. S. Han, *Adv. Mater.* **29**(17), 1605854 (2017).
- 11 A. Maali and B. Bhushan, *Philos. Trans. R. Soc., A* **370**(1967), 2304–2320 (2012).
- 12 J. A. Thomas and A. J. McGaughey, *Nano Lett.* **8**(9), 2788–2793 (2008).

- ¹³K. Falk, F. Sedlmeier, L. Joly, R. R. Netz, and L. Bocquet, *Nano Lett.* **10**(10), 4067–4073 (2010).
- ¹⁴S. K. Kannam, B. Todd, J. S. Hansen, and P. J. Davis, *J. Chem. Phys.* **136**(2), 024705 (2012).
- ¹⁵W. Xiong, J. Z. Liu, M. Ma, Z. Xu, J. Sheridan, and Q. Zheng, *Phys. Rev. E* **84**(5), 056329 (2011).
- ¹⁶A. Sam, R. Hartkamp, S. K. Kannam, and S. P. Sathian, *Nanotechnology* **29**(48), 485404 (2018).
- ¹⁷A. T. Celebi, M. Barisik, and A. Beskok, *J. Chem. Phys.* **147**(16), 164311 (2017).
- ¹⁸J. Zielkiewicz, *J. Chem. Phys.* **123**(10), 104501 (2005).
- ¹⁹G. Guevara-Carrion, J. Vrabec, and H. Hasse, *J. Chem. Phys.* **134**(7), 074508 (2011).
- ²⁰M. A. González and J. L. Abascal, *J. Chem. Phys.* **132**(9), 096101 (2010).
- ²¹S. Tazi, A. Boğan, M. Salanne, V. Marry, P. Turq, and B. Rotenberg, *J. Phys.: Condens. Matter* **24**(28), 284117 (2012).
- ²²G. S. Fanourgakis, J. Medina, and R. Prosimti, *J. Phys. Chem. A* **116**(10), 2564–2570 (2012).
- ²³S. Balasubramanian, C. J. Mundy, and M. L. Klein, *J. Chem. Phys.* **105**(24), 11190–11195 (1996).
- ²⁴B. Hess, *J. Chem. Phys.* **116**(1), 209–217 (2002).
- ²⁵F. Müller-Plathe, *Phys. Rev. E* **59**(5), 4894 (1999).
- ²⁶A. Russo, M. A. Durán-Olivencia, S. Kalliadasis, and R. Hartkamp, *J. Chem. Phys.* **150**(21), 214705 (2019).
- ²⁷Y. Song and L. L. Dai, *Mol. Simul.* **36**(7–8), 560–567 (2010).
- ²⁸S. Yongli, S. Minhua, C. Weidong, M. Congxiao, and L. Fang, *Comput. Mater. Sci.* **38**(4), 737–740 (2007).
- ²⁹T. Chen, B. Smit, and A. T. Bell, *J. Chem. Phys.* **131**(24), 246101 (2009).
- ³⁰R. Hartkamp, S. Bernardi, and B. D. Todd, *J. Chem. Phys.* **136**(6), 064105 (2012).
- ³¹Y. Mao and Y. Zhang, *Chem. Phys. Lett.* **542**, 37–41 (2012).
- ³²E. J. Wensink, A. C. Hoffmann, P. J. van Maaren, and D. van der Spoel, *J. Chem. Phys.* **119**(14), 7308–7317 (2003).
- ³³J. Backer, C. Lowe, H. Hoefsloot, and P. Iedema, *J. Chem. Phys.* **122**(15), 154503 (2005).
- ³⁴A. Markesteijn, R. Hartkamp, S. Luding, and J. Westerweel, *J. Chem. Phys.* **136**(13), 134104 (2012).
- ³⁵J. Ghorbanian and A. Beskok, *Microfluid. Nanofluid.* **20**(8), 121 (2016).
- ³⁶J. Ghorbanian, A. T. Celebi, and A. Beskok, *J. Chem. Phys.* **145**(18), 184109 (2016).
- ³⁷A. T. Celebi, M. Barisik, and A. Beskok, *Microfluid. Nanofluid.* **22**(1), 7 (2018).
- ³⁸S. K. Kannam, B. Todd, J. S. Hansen, and P. J. Davis, *J. Chem. Phys.* **135**(14), 144701 (2011).
- ³⁹L. Bocquet and J. Barrat, *Soft Matter* **3**(6), 685–693 (2007).
- ⁴⁰J. S. Hansen, B. Todd, and P. Davis, *Phys. Rev. E* **84**(1), 016313 (2011).
- ⁴¹B. Ramos-Alvarado, S. Kumar, and G. Peterson, *Phys. Rev. E* **93**(2), 023101 (2016).
- ⁴²N. V. Priezjev and S. M. Troian, *Phys. Rev. Lett.* **92**(1), 018302 (2004).
- ⁴³V. P. Sokhan and N. Quirke, *Phys. Rev. E* **78**(1), 015301 (2008).
- ⁴⁴A. Boğan, B. Rotenberg, V. Marry, P. Turq, and B. Noetinger, *J. Phys. Chem. C* **115**(32), 16109–16115 (2011).
- ⁴⁵A. Boğan, V. Marry, B. Rotenberg, P. Turq, and B. Noetinger, *J. Phys. Chem. C* **117**(2), 978–985 (2013).
- ⁴⁶C. Herrero, T. Omori, Y. Yamaguchi, and L. Joly, *J. Chem. Phys.* **151**(4), 041103 (2019).
- ⁴⁷P. Mark and L. Nilsson, *J. Phys. Chem. A* **105**(43), 9954–9960 (2001).
- ⁴⁸W. L. Jorgensen, J. Chandrasekhar, J. D. Madura, R. W. Impey, and M. L. Klein, *J. Chem. Phys.* **79**(2), 926–935 (1983).
- ⁴⁹J. L. Abascal and C. Vega, *J. Chem. Phys.* **123**(23), 234505 (2005).
- ⁵⁰W. L. Jorgensen and J. D. Madura, *Mol. Phys.* **56**(6), 1381–1392 (1985).
- ⁵¹H. J. Berendsen, J. P. Postma, W. F. van Gunsteren, and J. Hermans, *Intermolecular Forces* (Springer, Dordrecht, 1991).
- ⁵²Y. Wu, H. L. Tepper, and G. A. Voth, *J. Chem. Phys.* **124**(2), 024503 (2006).
- ⁵³H. Berendsen, J. Grigera, and T. Straatsma, *J. Phys. Chem.* **91**(24), 6269–6271 (1987).
- ⁵⁴S. Miyamoto and P. A. Kollman, *J. Comput. Chem.* **13**(8), 952–962 (1992).
- ⁵⁵R. Qiao and N. R. Aluru, *J. Chem. Phys.* **118**(10), 4692–4701 (2003).
- ⁵⁶K. P. Travis, B. Todd, and D. J. Evans, *Phys. Rev. E* **55**(4), 4288 (1997).
- ⁵⁷V. Sokhan, D. Nicholson, and N. J. Quirke, *J. Chem. Phys.* **115**(8), 3878–3887 (2001).
- ⁵⁸S. Bernardi, B. Todd, and D. J. Searles, *J. Chem. Phys.* **132**(24), 244706 (2010).
- ⁵⁹E. Wagemann, E. Oyarzua, J. H. Walther, and H. A. Zambrano, *Phys. Chem. Chem. Phys.* **19**(13), 8646–8652 (2017).
- ⁶⁰A. Sam, S. K. Kannam, R. Hartkamp, and S. P. Sathian, *J. Phys. Chem.* **146**(23), 234701 (2017).
- ⁶¹A. Yacoby, *Nat. Phys.* **7**(12), 925 (2011).
- ⁶²I.-C. Yeh and M. L. Berkowitz, *J. Chem. Phys.* **111**(7), 3155–3162 (1999).
- ⁶³T. Werder, J. H. Walther, R. Jaffe, T. Halicioglu, and P. Koumoutsakos, *J. Phys. Chem. B* **107**(6), 1345–1352 (2003).
- ⁶⁴Z. Li, Y. Wang, A. Kozbial, G. Shenoy, F. Zhou, R. McGinley, P. Ireland, B. Morganstein, A. Kunkel, and S. Surwade, *Nat. Mater.* **12**(10), 925 (2013).
- ⁶⁵M. Schrader, *J. Phys. Chem.* **84**(21), 2774–2779 (1980).
- ⁶⁶M. Tadros, P. Hu, and A. W. Adamson, *J. Colloid Interface Sci.* **49**(2), 184–195 (1974).
- ⁶⁷M. Luna, J. Colchero, and A. Baró, *J. Phys. Chem. B* **103**(44), 9576–9581 (1999).
- ⁶⁸A. H. Barber, S. R. Cohen, and H. D. Wagner, *Phys. Rev. Lett.* **92**(18), 186103 (2004).
- ⁶⁹J. Rafee, X. Mi, H. Gullapalli, A. V. Thomas, F. Yavari, Y. Shi, P. M. Ajayan, and N. A. Koratkar, *Nat. Mater.* **11**(3), 217 (2012).
- ⁷⁰C.-J. Shih, Q. H. Wang, S. Lin, K.-C. Park, Z. Jin, M. S. Strano, and D. Blankschtein, *Phys. Rev. Lett.* **109**(17), 176101 (2012).
- ⁷¹F. Taherian, V. Marcon, N. F. van der Vegt, and F. Leroy, *Langmuir* **29**(5), 1457–1465 (2013).
- ⁷²S. Wang, Y. Zhang, N. Abidi, and L. J. L. Cabrales, *Langmuir* **25**(18), 11078–11081 (2009).
- ⁷³Y. J. Shin, Y. Wang, H. Huang, G. Kalon, A. T. S. Wee, Z. Shen, C. S. Bhatia, and H. J. L. Yang, *Langmuir* **26**(6), 3798–3802 (2010).
- ⁷⁴F. M. Fowkes and W. D. Harkins, *J. Am. Chem. Soc.* **62**(12), 3377–3386 (1940).
- ⁷⁵I. Morcos, *J. Chem. Phys.* **57**(4), 1801–1802 (1972).
- ⁷⁶S. Plimpton, *J. Comput. Phys.* **117**(1), 1–19 (1995).
- ⁷⁷J. Medina, R. Prosimti, P. Villarreal, G. Delgado-Barrio, G. Winter, B. González, J. Aleman, and C. Collado, *J. Chem. Phys.* **388**(1–3), 9–18 (2011).
- ⁷⁸M. Suk and N. R. Aluru, *RSC Adv.* **3**(24), 9365–9372 (2013).
- ⁷⁹R. Qiao and N. R. Aluru, *Langmuir* **21**(19), 8972–8977 (2005).
- ⁸⁰R. Qiao and N. R. Aluru, *Phys. Rev. Lett.* **92**(19), 198301 (2004).
- ⁸¹R. Bhaduria and N. R. Aluru, *J. Chem. Phys.* **146**(18), 184106 (2017).
- ⁸²T. Q. Vo and B. Kim, *Sci. Rep.* **6**, 33881 (2016).
- ⁸³R. Hartkamp, A. Ghosh, T. Weinhart, and S. Luding, *J. Phys. Chem.* **137**(4), 044711 (2012).
- ⁸⁴T. A. Ho and A. Striolo, *J. Chem. Phys.* **138**(5), 054117 (2013).
- ⁸⁵J. Marti, J. Sala, and E. Guardia, *J. Mol. Liq.* **153**(1), 72–78 (2010).
- ⁸⁶T. A. Ho and A. Striolo, *Mol. Simul.* **40**(14), 1190–1200 (2014).
- ⁸⁷F. Sofos, T. Karakasidis, and A. Liakopoulos, *Int. J. Heat Mass Transfer* **52**(3–4), 735–743 (2009).
- ⁸⁸V. Prasad, S. K. Kannam, R. Hartkamp, and S. P. Sathian, *J. Chem. Phys.* **20**(23), 16005–16011 (2018).
- ⁸⁹M. K. Borg, D. A. Lockerby, K. Ritos, and J. M. Reese, *J. Membr. Sci.* **567**, 115–126 (2018).
- ⁹⁰N. Wei, X. Peng, and Z. Xu, *ACS Appl. Mater. Interfaces* **6**(8), 5877–5883 (2014).
- ⁹¹X. Gu and M. Chen, *Appl. Phys. Lett.* **99**(6), 063101 (2011).
- ⁹²P. Koumoutsakos, R. Jaffe, T. Werder, and J. Walther, in *2003 Nanotechnology Conference and Trade Show* (Computational Publications, San Francisco, California, USA, 2003), Vol. 1, pp. 148–151.